Available online at www.sciencedirect.com
ScienceDirect
Mathematics and Computers in Simulation 128 (2016) 1–12
MATHEMATICS AND COMPUTERS IN SIMULATION
www.elsevier.com/locate/matcom

Original articles

Numerical study of long-time Camassa–Holm solution behavior for soliton transport

C.H. Yu[a], Tony W.H. Sheu[b,c,*]

[a] Ocean College, Zhejiang University, 866 Yuhangtang Road, Hang HangZhou, Zhejiang, People's Republic of China
[b] Department of Engineering Science and Ocean Engineering, National Taiwan University, Taipei, Taiwan, ROC
[c] Taida Institute of Mathematical Sciences (TIMS), National Taiwan University, Taipei, Taiwan, ROC

Received 5 January 2012; accepted 1 January 2016
Available online 27 April 2016

Abstract

In this paper a three-step solution scheme is employed to numerically explore the long-time solution behavior of the Camassa–Holm equation. In the present $u - P - \alpha$ formation, we conduct modified equation analysis to eliminate several leading discretization error terms and perform Fourier analysis for minimizing the wave-like type of error. A three-point seventh-order spatially accurate combined compact upwind scheme is developed for the approximation of first-order derivative term. For the purpose of retaining Hamiltonian and multi-symplectic geometric structures in the non-dissipative Camassa–Holm equation, the adopted time integrator conserves symplecticity. Another main emphasis of this study is to numerically shed light on the scenario of the soliton transport.

Keywords: Camassa–Holm equation; Seventh-order spatially accurate; Symplecticity

1. Introduction

The completely integrable Camassa–Holm (CH) equation [2,3] has received considerable attention during the past three decades. Given an initial data falling into the Sobolev space $H^s(\Omega)$, CH equation is locally well-posed if $s > 3/2$ [5,7]. Popularity of this Cauchy problem arises from its rich geometric solution structure. Camassa–Holm equation developed for modeling the permanent wave has a global strong solution [8]. In addition, this equation permits blow-up solution that models the wave breaking [5,7]. Given an initial data of the $H^1(\Re)$ type, Camassa–Holm equation is also amenable to global weak solution [10,16].

* Corresponding author at: Department of Engineering Science and Ocean Engineering, National Taiwan University, Taipei, Taiwan, ROC. Tel.: +886 2 33665746; fax: +886 2 23929885.
E-mail address: twhsheu@ntu.edu.tw (T.W.H. Sheu).

http://dx.doi.org/10.1016/j.matcom.2016.01.008

The locally non-smooth time evolving CH solution is a direct result of the competition between the nonlinear compression uu_x, nonlinear dispersion uu_{xxx}, and possibly the mixed space–time derivative term u_{xxt}. An initially smooth solution may be compressed to generate a jump in finite time due to the embedded nonlinear terms [2]. In the presence of peakon solution, the CH solution computed at $\kappa = 0$ can exhibit even a discontinuous first derivative at the wave crest. At these peaks, any numerically introduced high-frequency dispersion error can considerably deteriorate the simulation quality [20].

To get a better understanding of the nonlinear and dispersive natures numerically in shallow water or in optical fiber, it is natural to apply a scheme which attains all the rich geometric structures. It is also desired to get the non-oscillatory solutions near the local peak and cusp solitons. How to preserve wave shape and speed subsequent to soliton collision and exhibit particle-like behavior in the CH equation is also essential.

The rest of this paper is organized as follows. Section 2 describes the nonlinear CH equation and some of its remarkable solution features. The classical CH equation is then transformed to its equivalent nonlinear system of equations that contains only the equation having the reduced differential order and the inhomogeneous Helmholtz equation. In the proposed solution algorithm, the nonlinear advection equation is first numerically approximated by the combined compact finite difference scheme. In Section 5 the CH equation will be solved for elucidating the long-time asymptotic solution behavior in the CH equation. Emphasis will be addressed on the transport of a single soliton and the interaction of two and three solitons. Finally, some concluding remarks will be drawn in Section 6.

2. Working equation and its fundamentals

In this paper, the following dispersive shallow water equation, known also as the Camassa–Holm (CH) equation, is studied in a domain $x \in R$ for the fluid velocity $u(x, t)$ at $t > 0$

$$u_t + 2\kappa u_x - u_{xxt} + 3uu_x = 2u_x u_{xx} + uu_{xxx}. \tag{1}$$

The coefficient shown above κ (>0) is the critical shallow water wave speed $(gh_0)^{1/2}$, where g and h_0 denote the gravity and undisturbed water depth. Two cases with $\kappa > 0$, which corresponds to have a smooth solitary wave, and $\kappa = 0$, which permits soliton with a sharp peak (or peakon) solution, are investigated. As κ approaches zero, CH solution becomes less smooth and may generate finally a discontinuity at the peak in the wave slope.

Eq. (1) can be represented in different mathematical forms. Define the momentum variable m as

$$m = u - u_{xx}. \tag{2}$$

This variable belongs to the class of Schwartz functions in the sense that $\int_{-\infty}^{\infty}(1 + |x|)|m(x)|dx < \infty$. One can then rewrite Eq. (1) in terms of m and the two Hamiltonians H_1 and H_2 as follows

$$m_t = -(2\kappa\partial + m\partial + \partial m)\frac{\delta H_1}{\delta_m} \tag{3}$$

$$m_t = -(\partial - \partial^3)\frac{\delta H_2}{\delta m}. \tag{4}$$

Because of the above two compatible descriptions, CH equation, by definition, has the bi-Hamiltonian structure for the Hamiltonians given below

$$H_1 = \frac{1}{2}\int mudx \tag{5}$$

$$H_2 = \frac{1}{2}\int u^3 + uu_x^2 + 2\kappa u^2 dx. \tag{6}$$

CH equation can be also represented by the classical Poisson Bracket form $m_t = \{m, H_1\}$, where $\{A, B\}$ is defined as

$$\{A, B\} = \int -\frac{\delta A}{\delta m}(2\kappa\partial + m\partial + \partial m)\frac{\delta B}{\delta m}dx. \tag{7}$$

One can rewrite Eq. (1) in terms of the eigenfunction ψ and its associated eigenvalue λ in the following Lax pair form

$$\psi_{xx} = \left(\frac{1}{4} + \lambda(m+\kappa)\right)\psi \tag{8}$$

$$\psi_t = \left(\frac{1}{2\lambda} - u\right)\psi_x + \frac{u_x}{2}\psi + \gamma\psi. \tag{9}$$

In the above, γ is an arbitrary constant. In other words, CH equation can be regarded as the compatibility condition between Eqs. (8) and (9) since $\partial_t\partial_{xx}\psi = \partial_{xx}\partial_t\psi$. Because of the available Lax pair, CH equation is completely integrable.

Given an initial condition $u_0(x, t = 0) \in H^1$, where H^1 denotes the Sobolev space, Eq. (1) has the following infinite sequence of conservation laws

$$(\partial - \partial^3)\frac{\delta H_n}{\delta m} = (2\kappa\partial + m\partial + \partial m)\frac{\delta H_{n-1}}{\delta m}. \tag{10}$$

In the above, $H_n(n = 0, \pm1, \pm2, \ldots,)$ denotes the Hamiltonian.

3. Solution algorithm for solving the CH equation

The third-order spatial derivative term and the mixed space–time derivative term in Eq. (1) were less explored numerically in comparison with the approximation of first-order derivative term. To avoid approximating these two higher-order derivative terms, the third-order CH equation is transformed to its equivalent system of equations containing only the first-order spatial and the temporal derivative terms by introducing the auxiliary variables given below. One can adopt first the momentum variable $m = u - u_{xx}$ to yield the following $u - m$ formulation [18].

$$m_t + um_x + 2u_x m = -2\kappa u_x. \tag{11}$$

Given the above action-angle variables, the evolution Eq. (1) in time can be used to model the linear transport of m at the constant speed. Note that CH equation becomes integrable provided that $\kappa > 0$ and $m(x, t = 0) + \kappa > 0$ [6,9]. As a result, the sum of κ and the Schwartz function m is positive for all t.

One can also transform the original CH equation to get the equivalent $u - P$ formulation given below [18]

$$u_t + uu_x = -P_x \tag{12}$$

$$P - P_{xx} = u^2 + \frac{1}{2}(u_x)^2 + 2\kappa u. \tag{13}$$

The above two sets of equations are normally solved subject to the prescribed periodic boundary condition. We have computationally assessed these two formulations and have drawn the conclusion that the $u - P$ formulation outperforms the $u - m$ formulation [18].

For the case with peakons and cuspons, it is inevitable to encounter discontinuity in the x-derivative of the solution. One must therefore avoid approximating $\partial u/\partial x$ shown on the right hand side of Eq. (12) and on the left-hand side of Eq. (13). To this end, Eq. (12) is rewritten to its equivalent equation given below

$$u_t + \frac{1}{2}(u^2)_x = -P_x. \tag{14}$$

To avoid computing the term u_x^2 in the inhomogeneous Helmholtz equation (13), we should replace u_x^2 by a term that is physically continuous even at a jump location in the wave crest. A good candidate is the one shown in the Hamiltonian H_2. The energy density given below is thus taken into account in the current simulation of CH equation [4,13]

$$\alpha = u^2 + (u_x)^2. \tag{15}$$

One can then easily derive the following transport equation for α in a conservative form as

$$\alpha_t + (u\alpha)_x = -Q_x \tag{16}$$

where $Q = 2Pu - u^3 - 2\kappa u^2$.

In summary, the set of equations used to avoid dealing with the computationally challenging terms u_{xxx}, u_{xxt} and u_x (in case of a non-smooth solution) is as follows

$$u_t + \frac{1}{2}(u^2)_x = -P_x \tag{17}$$

$$P - P_{xx} = u^2/2 + \alpha/2 + 2\kappa u \tag{18}$$

$$\alpha_t + (u\alpha)_x = -Q_x. \tag{19}$$

Within each $\Delta t (\equiv t_{n+1} - t_n)$, the solution u^{n+1} will be computed iteratively from u^n as follows. Given the time-accurate convergent solution for u and α at $t_n = n\Delta t$, we compute P from Eq. (18) and then the solution u from Eq. (17). This is followed by computing $Q(=2Pu - u^3 - 2\kappa u^2)$ and then α from Eq. (19). This process of calculations will be terminated until the criterion $\max\{|u^{k+1} - u^k|, |\alpha^{k+1} - \alpha^k|\} \le \varepsilon$ (the user's specified tolerance) is satisfied.

4. Numerical schemes

For approximating the time-dependent differential equation (17), in this study the classical semi-discretization method is adopted. The time derivative term will be approximated before approximating the spatial derivative terms.

4.1. Symplectic scheme for the time derivative term

Since Eq. (1) has a multi-symplectic structure, to get a long-term accurate solution the time-stepping scheme cannot be arbitrarily applied. In other words, a symplectic structure-preserving numerical integrator should be adopted to conserve symplecticity for the calculation of the currently investigated Hamiltonian differential system. The sixth-order accurate symplectic Runge–Kutta scheme [15] is chosen in this study to carry out a long-time integration of the non-dissipative CH equation:

$$u^{(1)} = u^n + \Delta t \left[\frac{5}{36} F^{(1)} + \left(\frac{2}{9} + \frac{2\tilde{c}}{3} \right) F^2 + \left(\frac{5}{36} + \frac{\tilde{c}}{3} \right) F^3 \right] \tag{20}$$

$$u^{(2)} = u^n + \Delta t \left[\left(\frac{5}{36} - \frac{5\tilde{c}}{12} \right) F^{(1)} + \frac{2}{9} F^{(2)} + \left(\frac{5}{36} + \frac{5\tilde{c}}{12} \right) F^{(3)} \right] \tag{21}$$

$$u^{(3)} = u^n + \Delta t \left[\left(\frac{5}{36} - \frac{\tilde{c}}{3} \right) F^{(1)} + \left(\frac{2}{9} - \frac{2\tilde{c}}{3} \right) F^{(2)} + \frac{5}{36} F^{(3)} \right] \tag{22}$$

$$u^{n+1} = u^n + \Delta t \left[\frac{5}{18} F^{(1)} + \frac{4}{9} F^{(2)} + \frac{5}{18} F^{(3)} \right] \tag{23}$$

where $\tilde{c} = \sqrt{3/5}/2$ and $F^{(i)} = F(u^{(i)}, \bar{P}^{(i)})$, $i = 1, 2, 3$.

In this applied symplectic Runge–Kutta method for the calculation of u^{n+1}, Eqs. (20)–(22) are solved implicitly for $u^{(1)}$, $u^{(2)}$ and $u^{(3)}$. We can then solve the Helmholtz equation (18) to get $P^{(1)}$, $P^{(2)}$ and $P^{(3)}$. Upon reaching the prescribed convergence criteria (10^{-9} in the current study), the solution u^{n+1} and then the solution $\bar{P}^{n+1}$ can be calculated.

4.2. Three-point seventh-order accurate upwinding combined compact difference (UCCD7) scheme

In the following, the combined compact upwinding scheme will be developed for the approximation of the first-order derivative term. At each interior grid point, ϕ_x, ϕ_{xx} and ϕ_{xxx} are all considered as the working variables so as to get the spectral-like resolution. Take $\phi = u$ as an example, the non-centered combined compact scheme will be presented in a three-point grid stencil for the approximation of $\frac{\partial \phi}{\partial x}$, $\frac{\partial^2 \phi}{\partial x^2}$ and $\frac{\partial^3 \phi}{\partial x^3}$ at the grid points i and $i \pm 1$

$$\left.\frac{\partial \phi}{\partial x}\right|_i + a_1 \left.\frac{\partial \phi}{\partial x}\right|_{i-1} + h \left(b_1 \left.\frac{\partial^2 \phi}{\partial x^2}\right|_{i-1} + b_2 \left.\frac{\partial^2 \phi}{\partial x^2}\right|_i + b_3 \left.\frac{\partial^2 \phi}{\partial x^2}\right|_{i+1} \right) + h^2 \left(c_1 \left.\frac{\partial^3 \phi}{\partial x^3}\right|_{i-1} + c_3 \left.\frac{\partial^3 \phi}{\partial x^3}\right|_{i+1} \right) = \frac{1}{h}(d_1 \phi_{i-1} + d_2 \phi_i + d_3 \phi_{i+1}) \tag{24}$$

$$\left.\frac{\partial^2\phi}{\partial x^2}\right|_i + \frac{1}{h}\left(-\frac{29}{16}\left.\frac{\partial\phi}{\partial x}\right|_{i-1} + \frac{29}{16}\left.\frac{\partial\phi}{\partial x}\right|_{i+1}\right) + \left(-\frac{5}{16}\left.\frac{\partial^2\phi}{\partial x^2}\right|_{i-1} - \frac{5}{16}\left.\frac{\partial^2\phi}{\partial x^2}\right|_{i+1}\right)$$
$$+ h\left(-\frac{1}{48}\left.\frac{\partial^3\phi}{\partial x^3}\right|_{i-1} + \frac{1}{48}\left.\frac{\partial^3\phi}{\partial x^3}\right|_{i+1}\right) = \frac{1}{h^2}(4\phi_{i-1} - 8\phi_i + 4\phi_{i+1}) \tag{25}$$

$$\left.\frac{\partial^3\phi}{\partial x^3}\right|_i + \frac{1}{h^2}\left(-\frac{105}{16}\left.\frac{\partial\phi}{\partial x}\right|_{i-1} - \frac{105}{16}\left.\frac{\partial\phi}{\partial x}\right|_{i+1}\right) + \frac{1}{h}\left(-\frac{15}{8}\left.\frac{\partial^2\phi}{\partial x^2}\right|_{i-1} + \frac{15}{8}\left.\frac{\partial^2\phi}{\partial x^2}\right|_{i+1}\right)$$
$$+ \left(-\frac{3}{16}\left.\frac{\partial^3\phi}{\partial x^3}\right|_{i-1} - \frac{3}{16}\left.\frac{\partial^3\phi}{\partial x^3}\right|_{i+1}\right) = \frac{1}{h^3}\left(\frac{105}{16}\phi_{i-1} - \frac{105}{16}\phi_{i+1}\right). \tag{26}$$

Both of the second-order derivative term $\partial^2\phi/\partial x^2$ and the third-order derivative term $\partial^3\phi/\partial x^3$ are approximated by the central schemes. These coefficients are determined simply by applying Taylor series expansions for eliminating their respective leading truncation error terms in the derived modified equations. The resulting formal accuracy orders become eighth-order and sixth-order, respectively [14].

Determination of the eight weighting coefficients in (24) is started by performing Taylor series expansion on ϕ_{i-1}, ϕ_{i+1}, $\frac{\partial\phi}{\partial x}|_{i-1}$, $\frac{\partial\phi}{\partial x}|_i$, $\frac{\partial^2\phi}{\partial x^2}|_{i-1}$, $\frac{\partial^2\phi}{\partial x^2}|_i$, $\frac{\partial^2\phi}{\partial x^2}|_{i+1}$, $\frac{\partial^3\phi}{\partial x^3}|_{i-1}$ and $\frac{\partial^3\phi}{\partial x^3}|_{i+1}$ with respect to ϕ_i. The leading eight truncation errors in the derived modified equation are eliminated to get the following set of algebraic equations

$$d_1 + d_2 + d_3 = 0 \tag{27}$$
$$-a_1 - d_1 + d_3 = 1 \tag{28}$$
$$2a_1 + d_1 + d_3 - 2b_1 - 2b_2 - 2b_3 = 0 \tag{29}$$
$$d_1 - d_3 - 6b_1 + 6b_3 + 6c_1 + 6c_3 + 3a_1 = 0 \tag{30}$$
$$d_1 + d_3 - 12b_1 - 12b_3 + 24c_1 - 24c_3 + 4a_1 = 0 \tag{31}$$
$$d_1 - d_3 - 20b_1 + 20b_3 + 60c_1 + 60c_3 + 5a_1 = 0 \tag{32}$$
$$d_1 + d_3 - 30b_1 - 30b_3 + 120c_1 - 120c_3 + 6a_1 = 0 \tag{33}$$
$$d_1 - d_3 - 42b_1 + 42b_3 + 210c_1 + 210c_3 + 7a_1 = 0. \tag{34}$$

One more algebraic equation is needed for us to uniquely determine all the nine introduced coefficients shown in (24) for the approximation of ϕ_x. Our strategy of maximizing dispersive accuracy is to match the numerical modified (or scaled) wavenumber with its analytical counterpart [19]. To this end, the following Fourier transform and its inverse of ϕ_x is applied

$$\tilde{\phi}(\beta) = \frac{1}{2\pi}\int_{-\infty}^{+\infty}\phi(x)e^{-\mathbf{i}\beta x}dx \tag{35}$$
$$\phi(x) = \int_{-\infty}^{+\infty}\tilde{\phi}(\beta)e^{\mathbf{i}\beta x}d\beta. \tag{36}$$

Note that the notation $\mathbf{i}$ shown above is equal to $\sqrt{-1}$.

In the chosen three-point grid stencil, the high-order upwinding compact scheme is developed by performing the Fourier transform on each term shown in Eqs. (24)–(26). The expressions of the actual (or exact) wavenumber β for these equations can be derived as follows

$$\mathbf{i}\beta h(a_1\exp(-\mathbf{i}\beta h) + 1) \simeq (d_1\exp(-\mathbf{i}\beta h) + d_2 + d_3\exp(\mathbf{i}\beta h)) - (\mathbf{i}\beta h)^2$$
$$\times (b_1\exp(-\mathbf{i}\beta h) + b_2 + b_3\exp(\mathbf{i}\beta h)) - (\mathbf{i}\beta h)^3(c_1\exp(-\mathbf{i}\beta h) + c_3\exp(\mathbf{i}\beta h)) \tag{37}$$
$$\mathbf{i}\beta h\left(-\frac{29}{16}\exp(-\mathbf{i}\beta h) + \frac{29}{16}\exp(\mathbf{i}\beta h)\right) \simeq 4\exp(-\mathbf{i}\beta h) - 8 + 4\exp(\mathbf{i}\beta h) - (\mathbf{i}\beta h)^2$$
$$\times\left(-\frac{5}{16}\exp(-\mathbf{i}\beta h) + 1 - \frac{5}{16}\exp(\mathbf{i}\beta h)\right) - (\mathbf{i}\beta h)^3\left(-\frac{1}{48}\exp(-\mathbf{i}\beta h) + \frac{1}{48}\exp(\mathbf{i}\beta h)\right) \tag{38}$$

$$\mathbf{i}\beta h\left(-\frac{105}{16}\exp(-\mathbf{i}\beta h)-\frac{105}{16}\exp(\mathbf{i}\beta h)\right)\simeq\left(\frac{105}{16}\exp(-\mathbf{i}\beta h)-\frac{105}{16}\exp(\mathbf{i}\beta h)\right)-(\mathbf{i}\beta h)^2$$
$$\times\left(-\frac{15}{8}\exp(-\mathbf{i}\beta h)+\frac{15}{8}\exp(\mathbf{i}\beta h)\right)-(\mathbf{i}\beta h)^3\left(-\frac{3}{16}\exp(-\mathbf{i}\beta h)+1-\frac{3}{16}\exp(\mathbf{i}\beta h)\right). \tag{39}$$

In an approximation sense, the effective (or numerical) scaled wave numbers $\beta' h$, $\beta'' h$ and $\beta''' h$ are made to render the same expressions as those shown on the right-hand sides of Eqs. (37)–(39) [19]. As a result, $\beta' h$, $\beta'' h$ and $\beta''' h$ can be expressed as follows:

$$\mathbf{i}\beta' h(a_1\exp(-\mathbf{i}\beta h)+1)=d_1\exp(-\mathbf{i}\beta h)+d_2+d_3\exp(\mathbf{i}\beta h)$$
$$-(\mathbf{i}\beta'' h)^2(b_1\exp(-\mathbf{i}\beta h)+b_2+b_3\exp(\mathbf{i}\beta h))-(\mathbf{i}\beta''' h)^3(c_1\exp(-\mathbf{i}\beta h)+c_3\exp(\mathbf{i}\beta h)) \tag{40}$$
$$\mathbf{i}\beta' h\left(-\frac{29}{16}\exp(-\mathbf{i}\beta h)+\frac{29}{16}\exp(\mathbf{i}\beta h)\right)\simeq 4\exp(-\mathbf{i}\beta h)-8+4\exp(\mathbf{i}\beta h)-(\mathbf{i}\beta'' h)^2$$
$$\times\left(-\frac{5}{16}\exp(-\mathbf{i}\beta h)+1-\frac{5}{16}\exp(\mathbf{i}\beta h)\right)-(\mathbf{i}\beta''' h)^3\left(-\frac{1}{48}\exp(-\mathbf{i}\beta h)+\frac{1}{48}\exp(\mathbf{i}\beta h)\right) \tag{41}$$
$$\mathbf{i}\beta' h\left(-\frac{105}{16}\exp(-\mathbf{i}\beta h)-\frac{105}{16}\exp(\mathbf{i}\beta h)\right)\simeq\left(\frac{105}{16}\exp(-\mathbf{i}\beta h)-\frac{105}{16}\exp(\mathbf{i}\beta h)\right)-(\mathbf{i}\beta'' h)^2$$
$$\times\left(-\frac{15}{8}\exp(-\mathbf{i}\beta h)+\frac{15}{8}\exp(\mathbf{i}\beta h)\right)-(\mathbf{i}\beta''' h)^3\left(-\frac{3}{16}\exp(-\mathbf{i}\beta h)+1-\frac{3}{16}\exp(\mathbf{i}\beta h)\right). \tag{42}$$

By solving Eqs. (40)–(42), the expression of $\beta' h$ can be derived in terms of the complex functions.

In the numerical modified (or scaled) wavenumber $\beta' h$, its real and imaginary parts are responsible respectively for the dispersion error (phase error) and the dissipation error (amplitude error). To get a better dispersive accuracy for β', we demand that $\beta h \approx \Re[\beta' h]$ where $\Re[\beta h]$ denotes the real part of $\beta' h$. This means that the magnitude of the integrated error function $E(\beta)$ defined below should be a very small and positive magnitude over the chosen range of integration

$$E(\beta)=\int_{-\pi/2}^{\pi/2}[W(\beta h-\Re[\beta'(h)])]^2 d(\beta h). \tag{43}$$

The weighting function W in (43) is the denominator of $(\beta h-\Re[\beta h])$ [1].

To make the error function defined in $-\pi/2\le\beta h\le\pi/2$ to be positive and minimum, the extreme condition $\partial E/\partial d_1=0$ is performed to minimize the numerical wavenumber error in Fourier analysis. The resulting constraint equation will be solved together with another eight previously derived algebraic equations derived from the modified equation analysis. This approach enables us not only to get a higher dissipation accuracy but also an improved dispersion accuracy. The resulting nine introduced unknowns can be uniquely determined as $a1=1.1875$, $b1=0.23643236$, $b2=-0.27774699$, $b3=-0.01356764$, $c1=0.01894044$, $c3=0.00189289$, $d1=-2.33613227$, $d2=2.48476453$ and $d3=-0.14863227$. The upwinding scheme developed above in a stencil of three grid points $i-1$, i and $i+1$ for $\partial\phi/\partial x=0$ has the spatial accuracy order of seventh because of the following derived modified equation

$$\frac{\partial\phi}{\partial x}=\left.\frac{\partial\phi}{\partial x}\right|_{exact}-0.65175737\times10^{-5}h^7\frac{\partial^8\phi}{\partial x^8}+0.81653294\times10^{-7}h^9\frac{\partial^{10}\phi}{\partial x^{10}}+H.O.T. \tag{44}$$

When $u<0$, we can similarly derive the following non-centered combined compact scheme in a three-point grid stencil containing the grid points i and $i\pm1$

$$\left.\frac{\partial\phi}{\partial x}\right|_i+1.1875\left.\frac{\partial\phi}{\partial x}\right|_{i-1}+h\left(0.01356764\left.\frac{\partial^2\phi}{\partial x^2}\right|_{i-1}+0.27774699\left.\frac{\partial^2\phi}{\partial x^2}\right|_i-0.23643236\left.\frac{\partial^2\phi}{\partial x^2}\right|_{i+1}\right)$$
$$+h^2\left(0.00189289\left.\frac{\partial^3\phi}{\partial x^3}\right|_{i-1}+0.01894044\left.\frac{\partial^3\phi}{\partial x^3}\right|_{i+1}\right)$$
$$=\frac{1}{h}(0.14863227\phi_{i-1}-2.48476453\phi_i+2.33613227\phi_{i+1}). \tag{45}$$

For developing an efficient and accurate numerical scheme for the inhomogeneous Helmholtz equation (13) or (18), the sixth-order accurate compact scheme presented in [18] will be adopted to get the following three-point equation.

$$P_{i+1} - \left(2 + h^2\bar{k} + \frac{1}{12}h^4\bar{k}^2 + \frac{1}{360}h^6\bar{k}^3\right) P_i + P_{i-1} = h^2 f_i + \frac{1}{12}h^4\left(\bar{k} f_i + \frac{\partial^2 f_i}{\partial x^2}\right) + \frac{1}{360}h^6\left(\bar{k}^2 f_i + \bar{k}\frac{\partial^2 f_i}{\partial x^2} + \frac{\partial^4 f_i}{\partial x^4}\right). \tag{46}$$

The corresponding modified equation for $\frac{\partial^2 P}{\partial x^2} - \bar{k}P = -(\frac{u^2}{2} + \frac{\alpha}{2} + 2\kappa u)(\equiv f)$ shown below confirms the proposed sixth-order accurate three-point stencil compact scheme

$$\frac{\partial^2 P}{\partial x^2} - \bar{k}P = f + \frac{h^6}{20160}\frac{\partial^8 P}{\partial x^8} + \frac{h^8}{1814400}\frac{\partial^{10} P}{\partial x^{10}} + \cdots + H.O.T. \tag{47}$$

5. Numerical results

In this study the CH equation will be solved for the case with the initial solution, which is not only sufficiently smooth but is also rapidly decaying at the two infinite ends $|x| \to \infty$. This investigated initial condition is also subjected to $u_0(x) - u_{0xx}(x) + \kappa > 0$ or $m_0 + \kappa > 0$ for all $x \in R$. Given this initial condition $u_0(x, t = 0)$, the CH solution $u(x, t)$ exists [6]. According to [12], there are four sectors in the (x, t) half-plane $t > 0$, in which the leading term of the longtime asymptotics of $u(x, t)$ behaves differently, depending on the magnitudes of $c = x/t$: (I) $c > 2$, (II) $c < 2$, (III) $-1/4 < c < 0$ and (IV) $c < -1/4$. In the solitonic solution sector (I), only the solution of the soliton type is seen. Upon passing over the narrow transition region $|x/t - 2|\, t^{2/3} < c$, oscillatory solution becomes exhibited. The first oscillatory region defined in [11] extends up to $x/t = 0$. In the sector between $-1/4 < x/t < 0$, another kind of oscillatory solution is described in [11]. Beyond the narrow region of the transition fan defined by $|x/t + 1/4|\, t^{2/3} < c$, CH solution becomes rapidly decaying in the sector $x/t < -1/4$. Only the case with a single soliton solution will be considered in this paper. The other three solutions in sectors (II)–(IV) will be our future study.

The proposed phase accurate and symplecticity optimized scheme will be validated first by solving the CH equation at $\kappa = 1.0$ in Section 5.1.1 and at $\kappa = 0.2$ in Section 5.1.2 for the single soliton solution. Soliton–soliton interaction problem will be solved in Section 5.2 and three-soliton interaction problem will be solved in Section 5.3. For the validation purpose, the following Hamiltonians will be plotted against time for each test problem

$$H_0 = \int u dx \tag{48}$$

$$H_1 = \frac{1}{2}\int (u^2 + u_x^2) dx = \int \alpha dx \tag{49}$$

$$H_2 = \frac{1}{2}\int (u^3 + u u_x^2 + 2\kappa u^2) dx = \int u\alpha dx. \tag{50}$$

5.1. One soliton problem

5.1.1. $\kappa = 1$

Given $k \in (0, 1/2)$ and κ, we have the corresponding single soliton solution given below in the "soliton" region, or sector (I)

$$u_{sol}(x - \kappa ct) = \frac{32\kappa k^2}{(1 - 4k^2)^2} \frac{\alpha(y(x - \kappa ct))}{(1 + \alpha(y(x - \kappa ct)))^2 + \frac{16k^2}{1-4k^2}\alpha(y(x - \kappa ct))}. \tag{51}$$

In the above, $\alpha(y) = \frac{\hat{\gamma}^2}{2k} e^{-2ky}$, $c = \frac{1}{2(1/4 - k^2)} \in (2, \infty)$, and $x = y + \log \frac{1 + \alpha(y)\frac{1+2k}{1-2k}}{1 + \alpha(y)\frac{1-2k}{1+2k}}$. The expression of $\hat{\gamma}$ is a function of $\frac{0.2-k}{0.2+k}$.

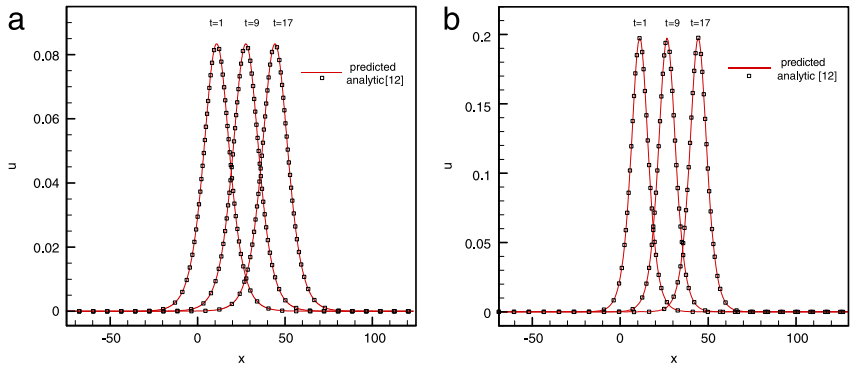

Fig. 1. Comparison of the predicted time-varying CH solutions in a domain of 256 grids at (a) $k = 0.1$, $\kappa = 1.0$ and $\hat{\gamma} = 0.1$; (b) $k = 0.15$, $\kappa = 1.0$ and $\hat{\gamma} = 0.02164$.

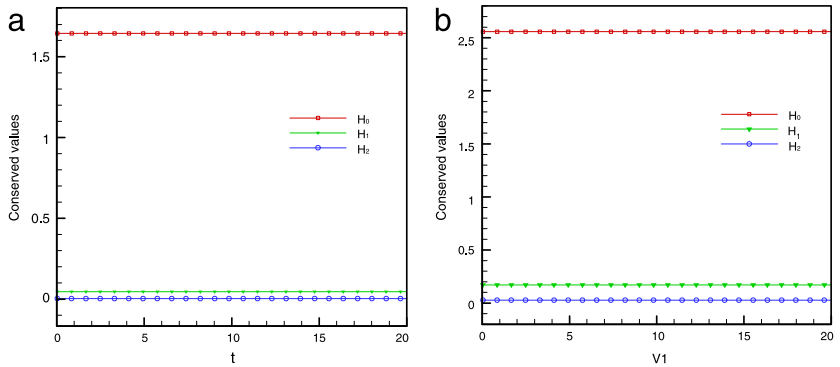

Fig. 2. The computed Hamiltonians H_0, H_1 and H_2 against time for the one soliton problem investigated at (a) $k = 0.1$ and $\kappa = 1.0$; (b) $k = 0.15$ and $\kappa = 1.0$.

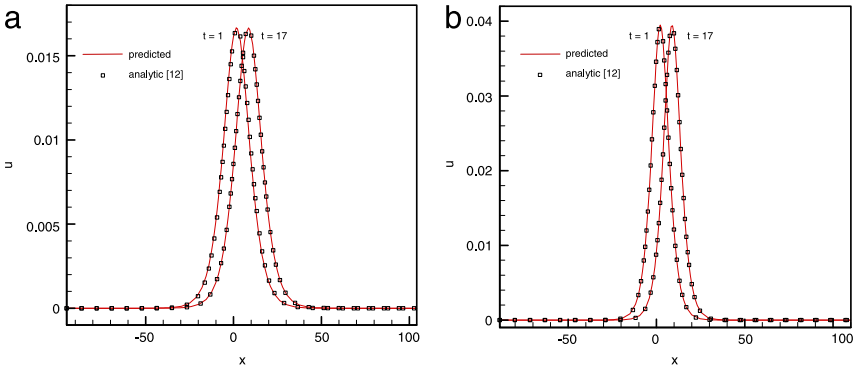

Fig. 3. Comparison of the time-varying CH solutions computed in a domain of 256 grids at (a) $k = 0.1, \kappa = 0.2$ and $\hat{\gamma} = 0.3333$; (b) $k = 0.15, \kappa = 0.2$ and $\hat{\gamma} = 0.1429$.

In Fig. 1(a)–(b), we can see that the time-evolving soliton solutions $u(x, t)$ predicted in 256 grids at $k = 0.1$ and 0.15 are compared excellently with the analytic results given in [12]. The Hamiltonians for the two investigated values of k are plotted respectively in Fig. 2(a)–(b). The unchanged Hamiltonians in time exhibit the globally non-dissipative solution behavior in the single soliton region.

5.1.2. $\kappa = 0.2$

In this section, the CH equation defined in $-400 \leq x \leq 400$ will be solved in 256 grids at $k = 0.1$ and $k = 0.15$. We make a direct comparison between our simulated results with the analytic results given in [12] for the CH solutions

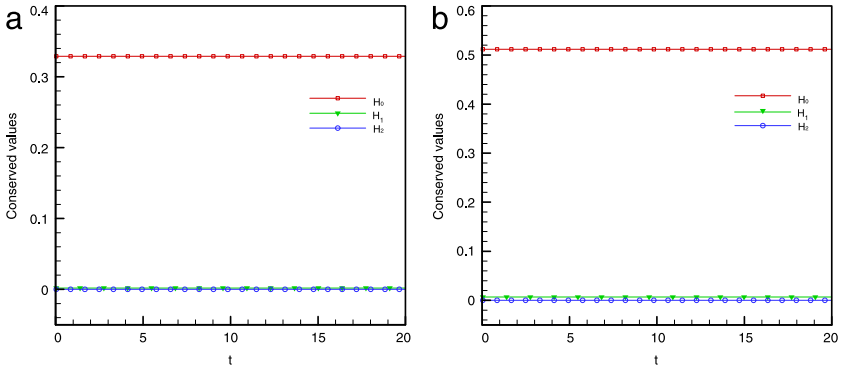

Fig. 4. The computed Hamiltonians H_0, H_1 and H_2 against time for the one soliton problem investigated at (a) $k = 0.1$ and $\kappa = 0.2$; (b) $k = 0.15$ and $\kappa = 0.2$.

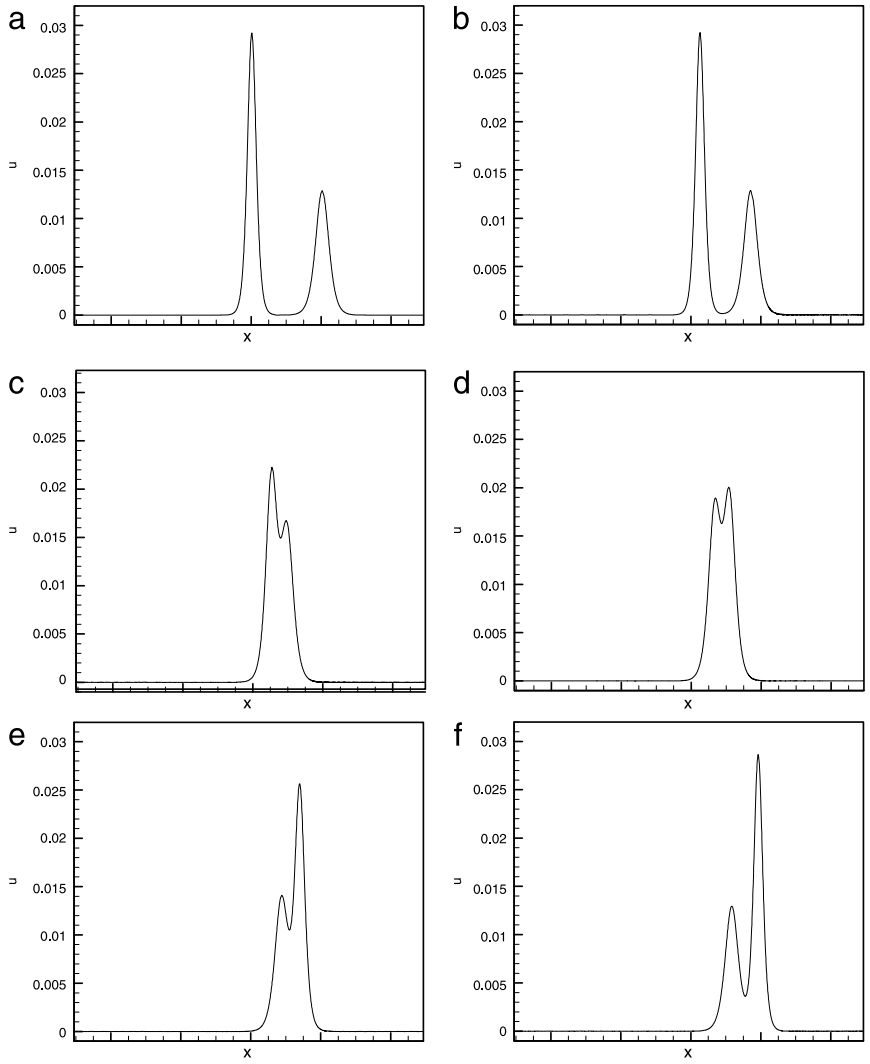

Fig. 5. The soliton–soliton solutions computed at different times in a domain of 2048 grids. (a) $t = 0$; (b) $t = 350$; (c) $t = 9900$; (d) $t = 10\,400$; (e) $t = 11\,400$; (f) $t = 12\,900$.

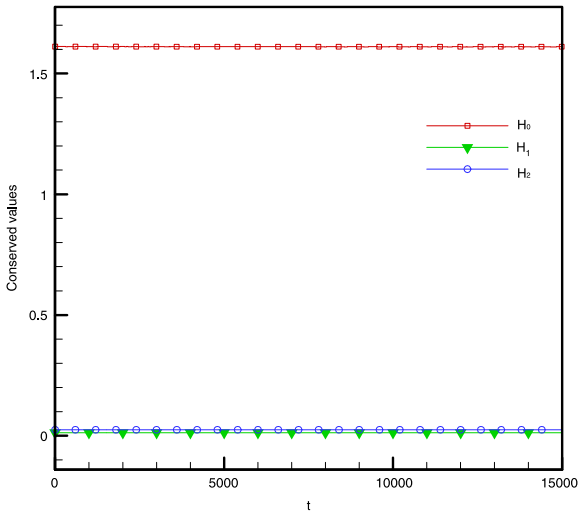

Fig. 6. Plot of the Hamiltonians H_0, H_1 and H_2 against time for the investigated soliton–soliton problem in Section 5.2.

predicted in sector (I) at $\kappa = 0.2$. Good agreement shown in Fig. 3(a)–(b) shows the proper application of the current prediction method to get the long-time solution behavior of the CH equation. We, as before, plot the computed values of the Hamiltonians in (48)–(50) against time at $k = 0.1$ and $k = 0.15$ in Fig. 4(a)–(b) to exhibit the globally non-dissipative soliton scenario.

5.2. Soliton–soliton interaction problem

Based on the proposed $u - P - \alpha$ formulation, Eq. (1) is then solved at $\kappa = 1.0$ for a pair of solitons. The initial two solitons shown in Fig. 5(a) are generated by Eq. (51) at $k = 0.04$ and $k = 0.06$. The resulting values of c for the two investigated values of k are 0.4171 and 0.2653.

The results for this soliton–soliton case are computed in a domain of 2048 uniform mesh points. Fig. 5(b)–(d) display the process of soliton collision at three different times. One can observe that the two-soliton solution regains its shape after the collision, resulting in only a phase shift. For the validation purpose, the computed values of the three unchanged Hamiltonians are also plotted against time in Fig. 6.

5.3. Three-soliton interaction problem

We then consider the case of three solitons propagating along the same direction [17]. The three-soliton solution for the CH equation (1) is represented in a parametric form given below [17]

$$u(y,t) = \frac{\partial}{\partial t}\ln\left(\frac{P}{Q}\right), \qquad x(y,t) = \frac{y}{k} + \ln\left(\frac{P}{Q}\right). \tag{52}$$

The above two functions P and Q are defined by

$$\begin{aligned} P(y,t) \;=\; & 1 + e^{\xi_1-\eta_1} + e^{\xi_2-\eta_2} + e^{\xi_3-\eta_3} + e^{\xi_1-\eta_1}e^{\xi_2-\eta_2}A_{12} + e^{\xi_1-\eta_1}e^{\xi_3-\eta_3}A_{13} \\ & + e^{\xi_2-\eta_2}e^{\xi_3-\eta_3}A_{23} + e^{\xi_1-\eta_1}e^{\xi_2-\eta_2}e^{\xi_3-\eta_3}A_{12}A_{13}A_{23} \end{aligned} \tag{53}$$

$$\begin{aligned} Q(y,t) \;=\; & 1 + e^{\xi_1+\eta_1} + e^{\xi_2+\eta_2} + e^{\xi_3+\eta_3} + e^{\xi_1+\eta_1}e^{\xi_2+\eta_2}A_{12} + e^{\xi_1+\eta_1}e^{\xi_3+\eta_3}A_{13} \\ & + e^{\xi_2+\eta_2}e^{\xi_3+\eta_3}A_{23} + e^{\xi_1+\eta_1}e^{\xi_2+\eta_2}e^{\xi_3+\eta_3}A_{12}A_{13}A_{23} \end{aligned} \tag{54}$$

where $\xi_i = p_i(y - \kappa c_i t)$, $c_i = \frac{2\kappa^2}{1-\kappa^2 p_i^2}$, $\eta_i = \ln(\frac{1+\kappa p_i}{1-\kappa p_i})$ for $i = 1, 2, 3$ and $A_{ij} = (\frac{p_i - p_j}{p_i + p_j})^2$, $1 \le i \le j \le 3$. The Camassa–Holm equation will be solved at $c_1 = 1.6$, $c_2 = 0.6$, $c_3 = 0.5$, $\kappa = (0.24)^4$ in a domain with the specified periodic boundary conditions.

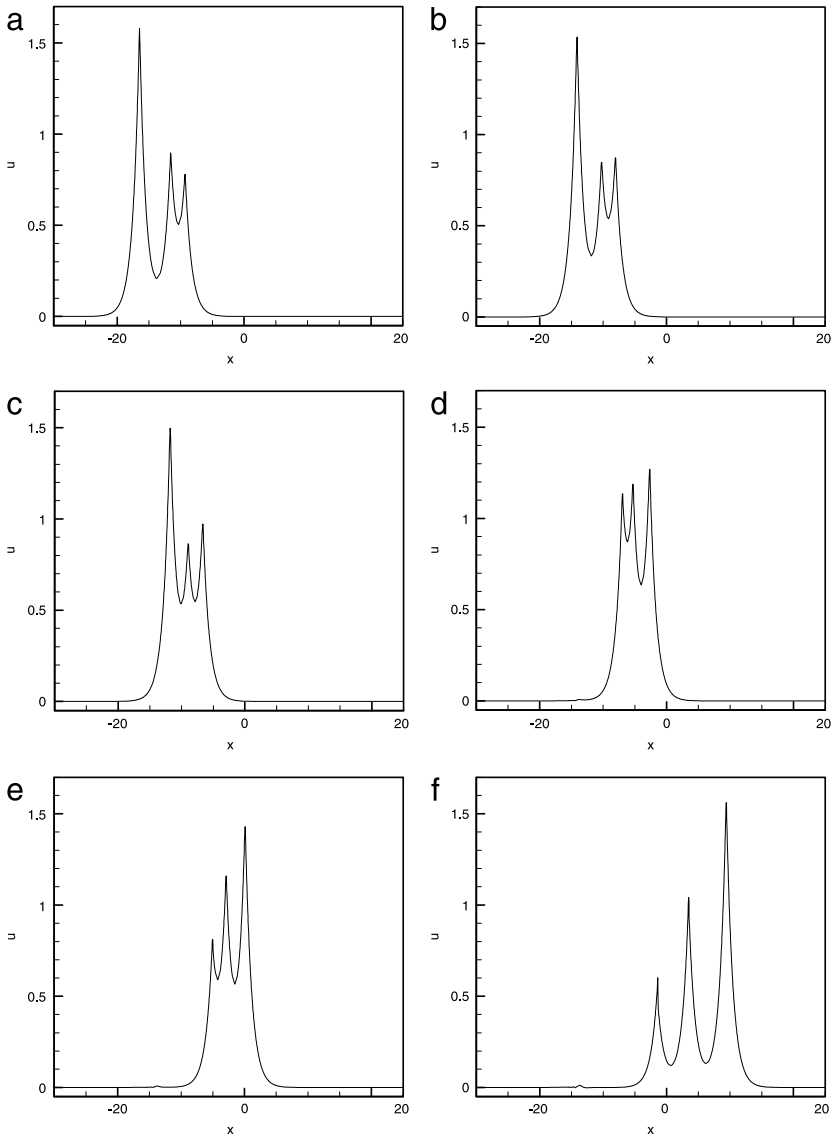

Fig. 7. The three-soliton solutions computed at different times in a domain of 4096 grids. (a) $t = 0.0$; (b) $t = 2.0$; (c) $t = 3.5$; (d) $t = 7.0$; (e) $t = 9.0$; (f) $t = 15.0$.

In Fig. 7, the time-evolving three-soliton solutions predicted in a domain of 4096 uniformly discretized grids are plotted. The switching scenario is clearly revealed without showing wave breaking. This three-soliton problem is thus known to have a global solution. In addition, the higher peakon is seen to move faster than the lower one. The Hamiltonians shown in Fig. 8 are unchanged all the time.

6. Concluding remarks

In the proposed $u - P - \alpha$ formulation for solving the Camassa–Holm equation, the time derivative term is approximated by the sixth-order accurate implicit symplectic Runge–Kutta scheme to retain the conserved properties in the non-dissipative Camassa–Holm equation. For the first-order spatial derivative terms shown in the equation, the dispersion error generated from the proposed seventh-order accurate upwind combined compact scheme is minimized. Based on the currently simulated results, we know that one-way propagation solitons proceed an elastic interaction in the non-dissipative CH equation.

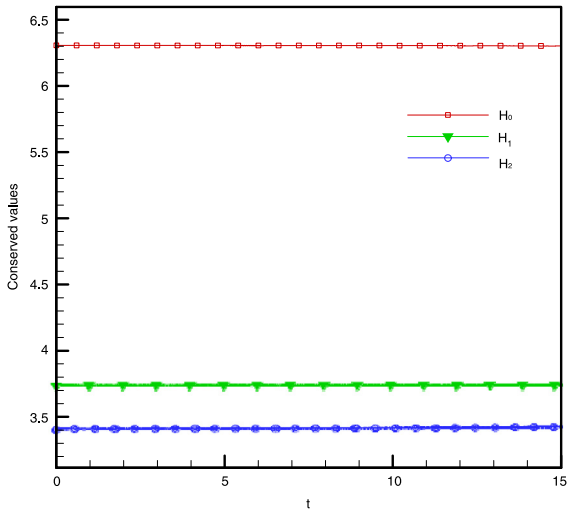

Fig. 8. Plot of the Hamiltonians H_0, H_1 and H_2 against time for the investigated three-soliton problem in Section 5.3.

Acknowledgment

This research is supported by National Science Council through the Grants NSC 98-2628-M-002-006 and 98-2811-E-002-006.

References

[1] G. Ashcroft, X. Zhang, Optimized prefactored compact schemes, J. Comput. Phys. 190 (2003) 459–477.
[2] R. Camassa, D.D. Holm, An integrable shallow water equation with peaked solitons, Phys. Rev. Lett. 71 (1993) 1661–1664.
[3] R. Camassa, D.D. Holm, J.M. Hyman, A new integrable shallow water equation, Adv. Appl. Mech. 31 (1994) 1–33.
[4] D. Cohen, B. Owren, X. Raynaud, Multi-symplectic integration of the Camassa–Holm equation, J. Comput. Phys. 227 (11) (2008) 5492–5512.
[5] A. Constantin, Existence of permanent and breaking waves for a shallow water equation: a geometric approach, Ann. Inst. Fourier (Grenoble) 50 (2000) 321–362.
[6] A. Constantin, On the scattering problem for the Camassa–Holm equation, Proc. R. Soc. Lond. Ser. A 457 (2001) 953–970.
[7] A. Constantin, J. Escher, Wave breaking for nonlinear shallow water equations, Acta Math. 181 (1998) 229–243.
[8] A. Constantin, J. Escher, Well-posedness, global existence, and blow-up phenomena for a periodic quasi-linear hyperbolic, Comm. Pure Appl. Math. 51 (1998) 475–504.
[9] A. Constantin, H.P. McKean, A shallow water equation on the circle, Comm. Pure Appl. Math. 52 (8) (1999) 949–982.
[10] A. Constantin, L. Molinet, Global weak solution for a shallow water equation, Comm. Math. Phys. 211 (2000) 45–61.
[11] A.B. De Monvel, A. Its, D. Shepelsky, Painlevé-type asymptotics for the Camassa–Holm equation, SIAM J. Math. Anal. 42 (4) (2010) 1854–1873.
[12] A.B. De Monvel, D. Shepelsky, G. Teschl, Long-time asymptotics for the Camassa–Holm equation, SIAM J. Math. Anal. 41 (4) (2009) 1559–1588.
[13] H. Holden, X. Raynaud, Global conservative solutions of the Camassa–Holm equation—a Lagrangian point of view, Comm. Partial Differential Equations 32 (10) (2006) 1511–1549.
[14] T. Nihei, K. Ishii, A fast solver of the shallow water equations on a sphere using a combined compact difference scheme, J. Comput. Phys. 187 (2003) 639–659.
[15] W. Oevel, M. Sofroniou, Symplectic Runge–Kutta schemes II: classification of symmetric method, Univ. of Paderborn, Germany, Preprint, 1997.
[16] A. Parker, Binary cuspon–soliton interactions, Chaos Solitons Fractals 41 (2009) 1531–1549.
[17] A. Parker, Y. Matsuno, The peakon limits of soliton solutions of the Camassa–Holm equation, J. Phys. Soc. Japan 75 (12) (2006) 124001.
[18] T.W.H. Sheu, P.H. Chiu, C.H. Yu, On the development of a high-order compact scheme for exhibiting the switching and dissipative solution natures in the Camassa–Holm equation, J. Comput. Phys. 230 (2011) 5399–5416.
[19] C.K.W. Tam, J.C. Webb, Dispersion-relation-preserving finite difference schemes for computational acoustics, J. Comput. Phys. 107 (1993) 262–281.
[20] Y. Xu, C.W. Shu, A local discontinuous Galerkin method for the Camassa–Holm equation, SIAM J. Numer. Anal. 46 (4) (2008) 1998–2021.